Available online at www.sciencedirect.com
ScienceDirect
Polymer 48 (2007) 763–777
polymer
www.elsevier.com/locate/polymer

The effect of temperature and annealing on the phase composition, molecular mobility and the thickness of domains in high-density polyethylene

Cristian Hedesiu [b,c], Dan E. Demco [c], Ralph Kleppinger [b], Alina Adams Buda [c], Bernhard Blümich [c], Klaas Remerie [a], Victor M. Litvinov [b,*]

[a] SABIC Europe BV, P.O. Box 319, 6160 AH, Geleen, The Netherlands
[b] DSM Research, Resolve, P.O. Box 18, 6160 MD Geleen, The Netherlands
[c] Institut für Technische Chemie und Makromolekulare Chemie, Rheinisch-Westfälische Technische Hochschule, Worringer Weg 1, D-52056 Aachen, Germany

Received 24 July 2006; received in revised form 30 October 2006; accepted 13 December 2006
Available online 17 December 2006

Abstract

Molecular mobility, the thickness of domains and the amount of rigid, semi-rigid, and soft fractions of high-density polyethylene (HDPE) were characterized as a function of temperature and annealing time using time- and frequency-domains proton solid-state NMR. These experiments established the temperature range for which the largest differences are observed in molecular mobility in crystalline phase, semi-rigid crystal–amorphous interface, and soft fraction of the amorphous phase allowing accurate determination of the phase composition and the thickness of these domains. The domain thickness, which was determined by NMR, is in good agreement to those measured by small-angle X-ray scattering (SAXS) and transmission electron microscopy (TEM) on the same sample. Changes in molecular mobility in the amorphous phase upon increasing temperature and annealing are discussed. It is shown that annealing is accompanied by structural reorganizations in the amorphous layer adjacent to the lamella surface causing a continuous shift of the interface towards the inner part of the amorphous regions and thus reducing the thickness of the amorphous layer. A recently introduced method was used for measuring the thickness of domains by a spin-diffusion NMR experiment with a double-quantum dipolar filter. The temperature dependence of the spin diffusivities is reported for the three phases of HDPE. For the first time results of spin-diffusion experiment performed by time-domain low-field NMR and frequency-domain high-field NMR are compared.

Keywords: Solid state NMR; SAXS; TEM

1. Introduction

The morphology of semi-crystalline polymers has important effects on the material properties including the mechanical performance [1,2]. A quantitative characterization of the phase composition and molecular mobility in semi-crystalline polymers is therefore of a great importance to advance our understanding of their properties. In this respect, the phase composition is probably one of the most important morphological parameters, mainly because the amorphous and crystalline phases exhibit vastly different behaviour and their relative contributions to the material properties should be accurately known. Traditionally, a two-phase model is used to describe the morphology of undeformed, melt-crystallized polyethylene (PE) and other semi-crystalline polymers [3,4]. The most common methods for crystallinity determination are X-ray diffraction, density measurement and differential scanning calorimetry. In general, different methods for crystallinity

* Corresponding author. Tel.: +31 46 4761256; fax: +31 46 4761200.
E-mail address: victor.litvinov@dsm.com (V.M. Litvinov).

0032-3861/$ - see front matter © 2006 Elsevier Ltd. All rights reserved.
doi:10.1016/j.polymer.2006.12.019

determination do not always yield the same results on exactly the same sample [5,6] because of the following reasons. (1) The complex morphology of semi-crystalline polymers requires different sets of assumptions for the analysis of the data recorded by different techniques. (2) The discrimination of the crystalline and amorphous phases is made on the basis of different characteristics, such as the enthalpy of melting (DSC), long-range periodicity (WAXD) and the specific volume (density analysis). (3) The two-phase model is simplified for the description of semi-crystalline polymers due to the presence of a crystal–amorphous interface, which can be detected either as crystalline or amorphous fraction depending on the method used [5]. Various experimental methods, such as neutron scattering, dielectric relaxation, calorimetry and solid-state NMR, show that a thin layer separates crystalline and amorphous phases, and the properties of this layer are intermediate between those for crystalline and amorphous phases [2,4,7,8]. Therefore, the term ''phase composition'' is perhaps more appropriate than simply ''crystallinity'' to emphasize the multi-phase nature of semi-crystalline polymers.

Solid-state NMR is one of the most informative techniques for characterization of molecular mobility and molecular scale heterogeneity in materials [9]. During the years, different solid-state NMR methods have been used for investigation of morphology and molecular mobility in PE. Proton wide-line NMR spectroscopy and relaxation experiments have been frequently applied to study the effect of the chemical structure, molar mass and temperature on the phase composition and molecular mobility [10–20]. At temperatures well above T_g of the amorphous phase, the T_2-relaxation decay and wide-line NMR spectra for PE can usually be decomposed into three components, which originate from a crystalline phase, a semi-rigid crystal–amorphous interface and a soft fraction of the amorphous phase. The intermediate phase has distinct dynamic properties and may not be considered as a true thermodynamic phase. Apparently, the definition of *an interface* or *a semi-rigid fraction of the amorphous phase* is more appropriate for this phase. ^{13}C NMR spectroscopy has provided more detailed information about molecular mobility in the different phases of PE than ^{1}H NMR because of the high phase selectivity of ^{13}C NMR exploring differences in the chemical shift for crystalline and amorphous phases [20–27]. Most of the ^{13}C NMR studies support the three-phase model of semi-crystalline PE. However, other studies suggested four types of structures with distinctly different molecular mobilities [22,27]: *two types of crystalline environment*, both with an *all trans* chain conformation – a more perfect one and one with ''twist'' defects, and *two types of chain fragments in the amorphous phase* – less mobile chain units mainly in the *trans* conformation rotating around trans chain axis, and more mobile chain fragments those mobility approaches isotropic tumbling. Detailed information about the nature of the molecular mobility in linear PE has been obtained by two-dimensional (2D) ^{13}C exchange NMR and ^{2}H wide-line NMR [24,28].

Despite numerous studies, the morphological origin of PE regions with different molecular mobilities is still a matter of discussion. Therefore the determination of the thickness of domains with distinctly different molecular mobility is of a substantial interest for better understanding of the morphology and relaxation properties of PE. Domain sizes in heterogeneous polymers [29,30] and polymer fibers [31–34] have been determined by proton NMR spin-diffusion experiments. Previous ^{1}H NMR spin-diffusion experiments have shown that the lamellae thickness of melt-crystallized PE and PE fibers varies in a wide range depending on the degree of the branching and the thermal history of sample [13,30]. It should be mentioned that *the thickness of the rigid fraction* in semi-crystalline polymers could differ from *the lamellae thickness* since some fraction of the amorphous phase adjacent to the lamellae surface can be largely immobilized and cause apparent increase in the lamellae thickness. The estimated thickness of the mobile amorphous fraction in PE ranges from 1 nm to 5 nm [13,27,30]. The morphology and phase characteristics of HDPE were also investigated by ^{13}C edited ^{1}H spin diffusion using a dipolar filter for filtering out the magnetization from the rigid phase [34]. The dimensions of 6.5 nm, 0.8–1.3 nm, and 5 nm were determined for the crystalline, intermediate, and amorphous phases, respectively. ^{13}C solid-state NMR methods offer certain advantages for the analysis of domain sizes in PE due to high phase selectivity [35,36]. However, quantitative studies of the phase composition, domain sizes, and molecular mobility in PE by ^{13}C NMR could suffer from a lack of accuracy due to very long ^{13}C T_1 value for the crystalline phase.

The high sensitivity of the proton NMR makes this method very attractive for characterization of crystallization kinetics [15], premelting behaviour [37], and quality control [38]. The main disadvantage of ^{1}H NMR for a phase analysis in PE is a lack of high selectivity regarding the crystalline and amorphous phases, if the experiments are performed at room temperature. A discrimination of these phases by proton NMR is made on the basis of differences in molecular mobility. Despite numerous ^{1}H NMR studies of PE, it is still not well known how annealing at elevated temperatures affects the phase composition and the thickness of the domains. To the best of our knowledge, the temperature dependence of the domain thickness was not studied by NMR so far, as well as the effect of annealing on the domain thickness.

Based on the above considerations, we aim to establish a reliable method for the analysis of the phase composition and domain sizes in HDPE using high-field proton wide-line NMR and low-field ^{1}H NMR transverse magnetization relaxation methods. By comparing the results of these two methods the performance of low-field NMR measurements for characterization of the domain sizes in semi-crystalline polymers can be validated. Furthermore, the effects of measurement temperature and annealing at elevated temperatures on the polymer morphology are studied in detail, as temperature may play a decisive role in the outcome of the measurements. Knowledge of the temperature effect will help to identity the temperature range for which the largest NMR difference between the different phases can be obtained, while ensuring high accuracy of the method by avoiding annealing. A recently developed NMR spin-diffusion experiment is applied for measuring the domain sizes [32,33,39]. This method, which explores double-quantum

dipolar filter [32,33,39–41], provides higher differences and, consequently, a more accurate analysis is possible. In order to evaluate the reliability of the NMR method, the results are compared with crystallinity and domain sizes determined for the same sample by SAXS and TEM.

2. Experimental section

2.1. Sample description and preparation

High-density polyethylene (HDPE) sample was obtained from SABIC Europe BV. The molar mass and molar mass distribution, as determined by size exclusion chromatography in 1,2,4-trichlorobenzene, were characterized by $M_n = 15 \times 10^3$ g/mol, $M_w = 78 \times 10^3$ g/mol, $M_z = 330 \times 10^3$ g/mol and $M_w/M_n = 5.2$. Four-millimeters thick compression-moulded plates were prepared by melting HDPE in a mould, first under atmospheric pressure at 180 °C with a subsequent pressure increase to 500 kPa. To create a homogeneous melt, the HDPE sample was kept in the mould for 15 min. Afterwards, the mould was cooled with cold water and the HDPE plates were annealed at 100 °C in an oven for 1 h followed by slow cooling to room temperature. For the annealing study, the sample was further annealed at different temperatures inside the NMR probe for 100 h.

2.2. DSC measurements

The DSC measurements were performed with a Perkin–Elmer DSC-7 at a heating rate of 10 °C/min. The melting peak and the melting enthalpy, which were determined from the first melting endotherm of the core part of the plate, were 136.1 °C and 229.5 kJ/kg, respectively. Slightly different values of 134.9 °C and 224.1 kJ/kg were obtained for the skin layer. The glass transition temperature for the amorphous phase of the HDPE sample was observed at −57 °C by a high performance DSC at a heating rate of 150 °C/min.

2.3. Transmission electron microscopy (TEM)

For recording transmission electron micrographs, the compression-moulded plate was trimmed at a temperature of −120 °C and stained for 24 h in a RuO_4 solution. Sections of 70 nm thick were obtained by slicing the sample with an ultramicrotom at −120 °C. Images were recorded with a Philips CM200 TEM at an acceleration voltage of 120 kV.

2.4. Small angle X-ray scattering

The small-angle X-rays scattering (SAXS) experiments were performed with a modified Kratky setup (entrance slit 40 μm, sample-detector distance 288 mm), attached to a sealed tube X-ray source (40 kV and 50 mA), providing line-focused, Ni-filtered CuK_α radiation (0.154 nm). The scattering signal was recorded using a Mbraun 50M position sensitive detector. Calibration of the data and subtraction of the transmission-weighted background signal yielded intensity profile $I(q)$, where $q = (4\pi/\lambda)\sin\vartheta$ (with λ, wavelength and 2ϑ, scattering angle). Desmearing of the slit-smeared intensity profiles $I(q)$ was performed with the FFSAXS software, using the infinite-slit approximation [42,43].

After subtracting contributions from liquid-like scattering $B(q)$ from the desmeared data [43], the linear correlation functions $G(r)$ were calculated via (inverse) Fourier transform according to

$$G(r) = \int_0^\infty [I(q) - B(q)]q^2\cos(qr)\mathrm{d}q. \tag{1}$$

The interpretation of the linear correlation function starts from the assumption of (more or less) regular stacked sheet-like crystalline domains with thickness t, occupying a volume fraction ϕ, that are separated by amorphous interlayer and thus yield a lamellar structure with periodicity L. The scattering power, Q, of such quasi-periodic assembly is

$$Q = \int_0^\infty I(q)q^2\mathrm{d}q \propto (\rho_c - \rho_a)^2\phi(1-\phi), \tag{2}$$

where ρ_c and ρ_a represent the electron densities of the crystalline and amorphous domains, respectively.

The latter is used to obtain the normalized correlation functions $\gamma(r)$ via

$$\gamma(r) = \frac{G(r)}{Q} \tag{3}$$

which is finally evaluated with respect to the characteristic dimensions of the quasi-periodic structure. The long period L was extracted from the position of the slide maximum of $\gamma(r)$, whereas the lamellar thickness was derived from the intersect of the autocorrelation triangle at $\gamma(A) = 0$ with

$$A = L_p\phi(1-\phi) = \mathrm{d}(1-\phi), \tag{4}$$

where ϕ represents the degree of crystallinity of the samples, estimated from the minimum value of the correlation function via

$$\gamma_{min} = \frac{\phi^2}{\left[\phi(1-\phi) - \frac{\sigma}{3L_p}\right]}. \tag{5}$$

2.5. NMR measurements and data analysis

The phase composition, the thickness of the domains, and the molecular mobility were studied with the help of three different solid-state ^{1}H NMR methods: wide-line NMR spectroscopy, transverse magnetization relaxation (T_2 relaxation) and spin-diffusion experiments. The experiments were performed with NMR spectrometers that operate at high and low strengths of the static magnetic field.

NMR experiments at high field were conducted with a Bruker DSX spectrometer operating at a proton resonance

frequency of 500.45 MHz. The data were collected for static samples at temperatures between room temperature and 120 °C. The duration of the 90° pulse was about 5 μs and the dwell time was set to 0.75 μs. A recycle delay of 5 s was used for all experiments. The experimental wide-line spectra were deconvoluted in three components using the Bruker WinFit program. The broad component of the spectra was approximated by a Gaussian function. This is a rough approximation of the actual line shape as shown below. The shape parameter ($\alpha = 0.5$) of the line with intermediate width (i.e. the interface) was between that of a Gaussian ($\alpha = 1$) and a Lorentzian ($\alpha = 0$). It is noted that the theoretical description of the line shape for the amorphous phase in semi-crystalline polymers is still under debate, which is in part due to complex morphology of these materials. The spectra fit has shown that the narrow component of the spectra that belongs to the amorphous fraction with high chain mobility can be well described by the Lorentzian line shape.

Spin-diffusion and T_2-relaxation experiments were performed for static samples on low-field NMR Bruker Minispec spectrometers NMS-120 and MQ-20. Both spectrometers operate at a proton resonance frequency of 19.6 MHz. The duration of the 90° pulse and the dead time were 2.8 μs and 7 μs, respectively. The dwell time was 0.5 μs. A BVT-3000 temperature controller assumed temperature stability better than 1 °C.

Three different pulse sequences were used with the low-field NMR spectrometers to measure accurately the decay of the ^{1}H transverse magnetization (T_2 decay) from both rigid and soft fractions of the sample: (1) the free induction decay (FID) after a 90° pulse excitation (SPE − single pulse excitation), i.e. $90°_x$–dead time − acquisition of the amplitude $A(t)$ of the transverse magnetization as a function of time t, (2) the solid-echo pulse sequence (SEPS), i.e. $90°_x$–t_{se}–$90°_y$–t_{se} − acquisition of the amplitude of the transverse magnetization $A(t)$, with $t_{se} = 10$ μs, and (3) the Hahn-echo pulse sequence (HEPS), i.e. $90°_x$–t_{He}–$180°_x$–t_{He} − acquisition of the amplitude of the echo maximum for variable value of t_{He}. The SPE and SEPS could cause systematic errors in the analysis of the phase composition in heterogeneous materials. The initial part of the FID is not detected after 90° pulse excitation because of the dead time of the receiver. Therefore, the knowledge of the shape of the transverse magnetization decay for the rigid phase is required for accurate deconvolution of the FID into components corresponding to different phases. The shape of the FID for the rigid fraction can be determined by the SEPS. The SEPS has the advantage of avoiding the dead time of the spectrometer. The amplitude of the transverse magnetization of the rigid and soft fraction is lower than the real one because of the following reasons: (1) the incomplete refocusing of the dipolar interactions for a dipolar network by the solid-echo [18,19], (2) molecular motions, the correlation time of which is comparable to the pulse spacing [18,19], and (3) the shift of the echo maximum caused by nonzero pulse width [18,19].

In order to estimate these systematic errors, the SEPS experiment was performed at different solid-echo times t_{se} for HDPE. It can be seen in Fig. 1 that the initial amplitude of the fast, $A(0)^r$, intermediate, $A(0)^i$, and long, $A(0)^l$, decay components has decreased with increasing t_{se}. Thus, the fraction of $A(0)^r$ is largely underestimated in the SEPS, which does not allow using this experiment for quantitative analysis of the phase composition, if the experiment is performed for one value of t_{se}. Extrapolation of the dependence $A(0)^r$, $A(0)^l$ and $A(0)^i$ on t_{se} to time $t_{se} = 0$ provides the absolute value of the amount of the rigid phase, as determined by a value of $A(0)^r/[A(0)^r + A(0)^i + A(0)^l]$. The extrapolated value coincides with that determined by a least-squares fit of the free induction decay (FID) after 90° pulse excitation (Fig. 1). Analysis of the solid-echo decay and FID shows the same shape of the fast decaying component approached by the Abragam shape (see Eq.(6)). Therefore, the 90° pulse excitation was finally used to record the FID for the quantitative analysis of the phase composition. An additional experiment with Hahn-echo pulse sequence was used in order to avoid the effect of the inhomogeneity of the magnetic field on the decay of $A(0)$.

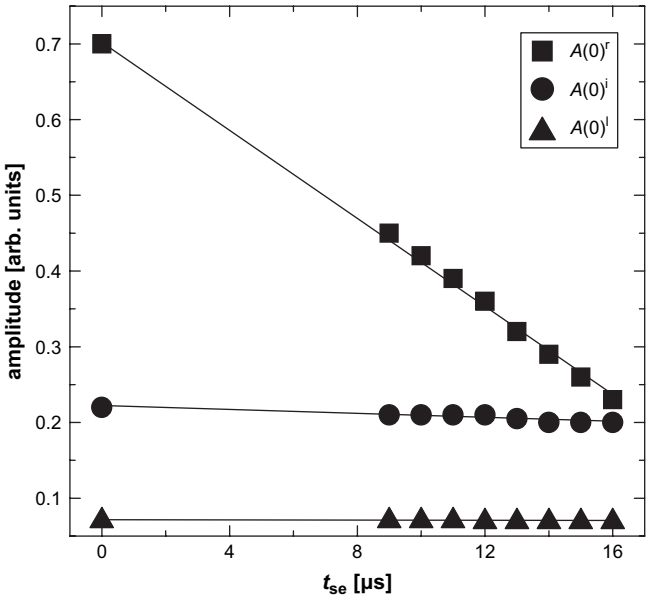

Fig. 1. The initial amplitude of the fast $A(0)^r$, intermediate $A(0)^i$ and slowly $A(0)^l$ decaying components of the transverse magnetization decay against the pulse spacing t_{se} in the SEPS. The amplitudes at $t_{se} = 0$ are determined from a least-squares analysis of FID measured after 90° pulse excitation. The NMR experiments are performed for HDPE at 100 °C.

The amplitude of the FID for times t longer than 200 μs is affected by the inhomogeneity of the magnetic field, which is due to the inhomogeneity of the permanent magnetic field B_o itself and B_o inhomogeneity within a sample volume that arises from an inhomogeneous magnetic susceptibility of the heterogeneous sample. By varying the inter-pulse spacing in the HEPS from 75 μs to 10 ms, the amplitude of the Hahn echo $A(t)$ is measured as a function of the time. The HEPS should be used for obtaining reliable information about the amount and the rate of the transverse magnetization relaxation of a soft fraction of HDPE. Whereas the FID recorded by SPE provides accurate information on the effective relaxation times and the amount of rigid- and semi-rigid HDPE fractions. The amplitude of the transverse magnetization, which is determined by the SPE and HEPS experiments, was the same in the time

interval from about 75 μs to 180 μs (see Fig. 6a). Therefore, the results of both experiments were combined in a single file.

The combined data file was fitted with a linear combination of the Abragam function [44] and two exponential functions:

$$A(t) = A(0)^{s}\exp\left[-\left(t/2T_2^{s}\right)^2\right][\sin(at)/at] + A(0)^{i}\exp\left[-\left(t/T_2^{i}\right)\right] + A(0)^{l}\exp\left[-\left(t/T_2^{l}\right)\right]. \quad (6)$$

The Abragam function [44] corresponds to the first term of Eq. (6). The parameter a depends on the distance between hydrogen atoms of the methylene group, and is related to the second and fourth van Vleck moments. The effective transverse relaxation time, T_2^{s}, for the rigid fraction is a measure of the second van Vleck moment, i.e. $M_2 = 1/(T_2^{s})^2$. The relative fraction of the relaxation components, $\{A(0)^{k}/[A(0)^{s} + A(0)^{i} + A(0)^{l}]\} \times 100\%$, where $k = $ s, i and l represents the relative amount of hydrogen atoms (mass fractions) of HDPE phases/fractions with different molecular mobility. Repeated experiments for the same sample indicated that the relative error of the relaxation parameters was about 2%.

2.6. Determination of the domain thickness by NMR spin-diffusion experiments

The majority of spin-diffusion investigations performed in the past used different types of dipolar filters that select mainly the signal from the domains with high molecular mobility [9,13,30,34,45–48]. Multiple-quantum coherences of dipolar coupled spins-1/2 nuclei in the solids [49,50] have also been exploited as a filter to separate different magnetization components in a spatially heterogeneous system [39–41]. The main advantage of multiple-quantum (MQ) dipolar filters is that, in combination with the dipolar filters of the mobile phase, one can gain more detailed information about complex polymer morphologies [32,33]. Moreover, to use this type of filter is more advantageous than a dipolar filter for mobile domains because the MQ filter allows a more accurate detection of the narrow line on the top of the broad one as compared to the detection of the broad line under the narrow signal, which is the case of the Goldman–Shen filter [9,46]. This is valid especially at short diffusion times when the intensity of one of the components is very small.

In the present study, proton double-quantum (DQ) build-up curves and spin-diffusion data were recorded. The spin-diffusion experiments consisted of a z-magnetization dipolar filter, a spin-diffusion period of duration t_d, and an acquisition period, as shown in Fig. 2. The dipolar filter excites double-quantum coherences and selects mainly the magnetization of rigid phase at short excitation times $t_{DQ} = 5$ μs [39]. The excitation/reconversion time τ, which corresponds to the maximum of the DQ build-up curve, was determined in a series of experiments with variable values of τ and t_d. The recycle delay was 3 s. The same parameters were used for the spin-diffusion experiments at low- and high-strength of the magnetic fields.

The FIDs recorded at low frequency and at different mixing times t_d were analysed with a least-squares fit program developed at DSM Research. In addition to fitting a single FID, the fit program can be also used to fit an array of FIDs measured at different mixing times (global fit). The global fit adjusts one T_2 value for each relaxation component of FIDs in the array providing the minimum standard deviation of residuals for all set of the data. The important improvement of the global fit, as compared with a separate fit of each FID, is the high reliability of the best-fit values of the relative fractions of the relaxation components even for their small values.

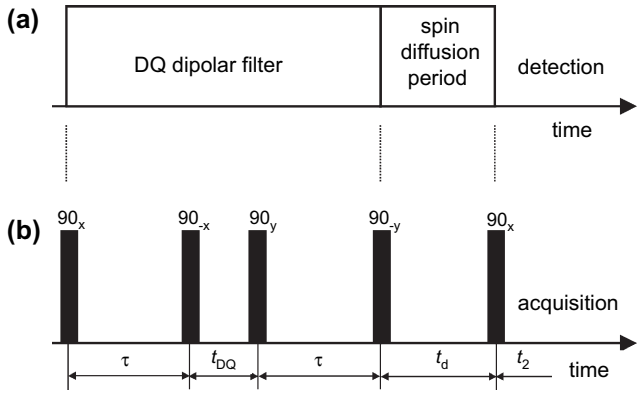

Fig. 2. (a) General scheme of spin-diffusion experiments using a double-quantum (DQ) dipolar filter. (b) Four-pulse double-quantum filter, which is followed by a 90°$_x$-detection pulse after the spin-diffusion time t_d in the spin-diffusion experiment.

The thickness of the rigid, semi-rigid and soft domains of HDPE was determined by a fit of the dependencies of the signal amplitudes for these fractions as a function of the mixing time. For this purpose, a one-dimensional (1D) analytical solution for the spin-diffusion equations was used [32,33,39]. It should be noted that the shape of the spin-diffusion curves could be affected by spin–lattice (T_1) relaxation. In the present study, the spin-diffusion process was nearly completed at the longest mixing time $t_d = 100$ ms, however, t_d being significantly shorter than T_1. Therefore, no T_1 correction of the spin-diffusion data was needed.

3. Results and discussion

3.1. Morphology of HDPE by TEM

The transmission electron micrograph of the sample shows stacked lamellar crystals (Fig. 3) that are separated by a thin amorphous layer. The estimated thickness of lamellae in the core part of the sample is 16 ± 2 nm. The thickness of the amorphous layer does not exceed 2–3 nm. The value of the L_p was determined directly by measuring the lamellae periodicity (in mm) on the TEM image and converting the obtained value to L_p using the scale of the TEM image. No advanced analysis of the TEM image has been performed.

3.2. Crystallinity and morphology by SAXS

The SAXS patterns reveal a maximum due to the long period (Fig. 4), which is a typical feature of semi-crystalline polymers. For HDPE, this can be interpreted in terms of a

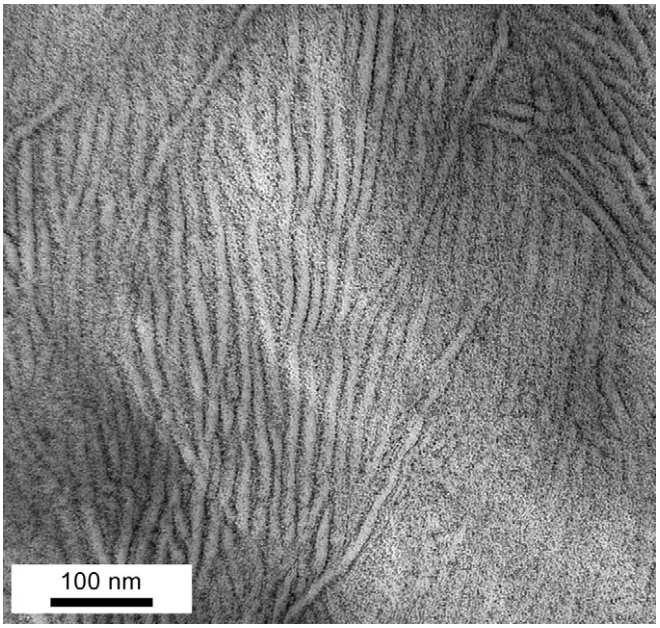

Fig. 3. TEM picture of a core part of a compression-moulded HDPE plate. The length of 100 nm is shown in the bottom left-down corner of the figure.

quasi-periodic, lamellar morphology as outlined in more detail above. The analysis of the one-dimensional electron density correlation function assumes the two-phase model, which cannot be strictly valid due to the presence of the interfacial layer, as will be shown below by NMR experiments. The long period L_p is estimated from the position of the first interference maximum, at about 0.038 nm^{-1} (Fig. 4), and from the normalized correlation function, which is shown in Fig. 5. According to these data, the long period is close to 25 nm, which is larger than the values obtained by TEM, i.e. $(18-19) \pm 2$ nm. It is noted that the L_p value can suffer from systematic errors due to the experimental set-up used.

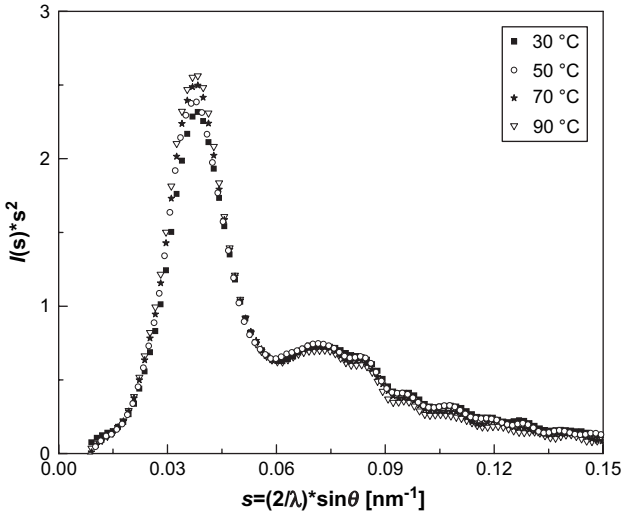

Fig. 4. One-dimensional scattering intensities $I_1(s) = I(s)*s^2$ recorded at various temperatures, indicating the maximum of the long period due to periodic stacking of crystalline lamellae.

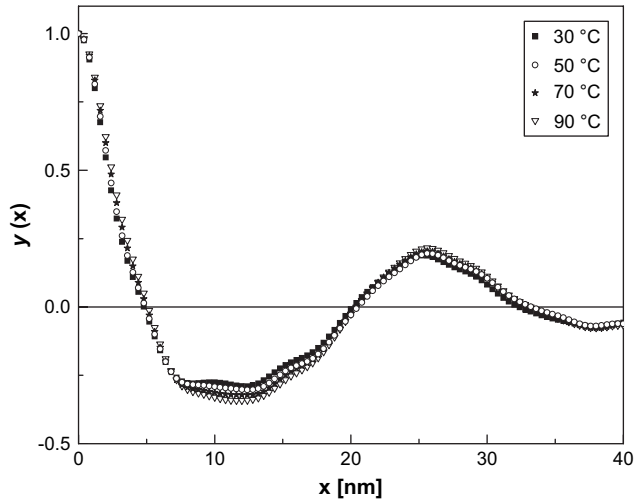

Fig. 5. Normalized linear correlation functions $\gamma(x)$ derived from the SAXS data shown in Fig. 4.

Based on the analysis of the correlation functions, the thickness of the crystalline domains is estimated to 17–18 nm, which is in good agreement with the value measured by TEM and NMR, as will be shown below. With the values of d and L_p from the correlation functions, the crystallinity is estimated to 68 ± 5 vol%. This value corresponds to a crystallinity in mass percent of 71 ± 5 wt%, which is calculated with the densities of the crystalline and amorphous phases of 0.99 g/cm^3 and 0.87 g/cm^3, respectively. It is suggested in this calculation that the density of an interfacial layer is given by the mean value of the densities for the crystalline and amorphous phases. SAXS experiments at different temperatures reveal almost the same long period, lamella thickness, and crystallinity in the temperature range from 30 °C to 90 °C.

3.3. Solid-state NMR study of the phase composition, molecular mobility, and domain thickness

3.3.1. Temperature dependence of the phase composition and chain mobility

The proton NMR free induction decay (FID) measured for HDPE at 100 °C is shown in Fig. 6a. The FID can be decomposed into three components. They are assigned to three fractions with different molecular mobility, the rigid – T_2^s, semi-rigid – T_2^i, and soft – T_2^l fractions, respectively [11,12,14,18]. The existence of three fractions with different molecular mobility is evidently shown by ^{1}H NMR spectra (Fig. 6b). Like the FID, the spectra can be deconvoluted into three components. Broad, intermediate and narrow lines originate from rigid, semi-rigid and soft fractions of HDPE, respectively. However, the quantitative analysis of FID and wide-line NMR spectra in terms of crystalline phase, crystal–amorphous interface and soft fraction of the amorphous phase can be complicated due to the following reasons. (1) To observe distinct differences in molecular mobility of the crystalline and amorphous phases, and consequently in the T_2 relaxation and the line width, the temperature of the sample should substantially exceed the dynamic glass transition

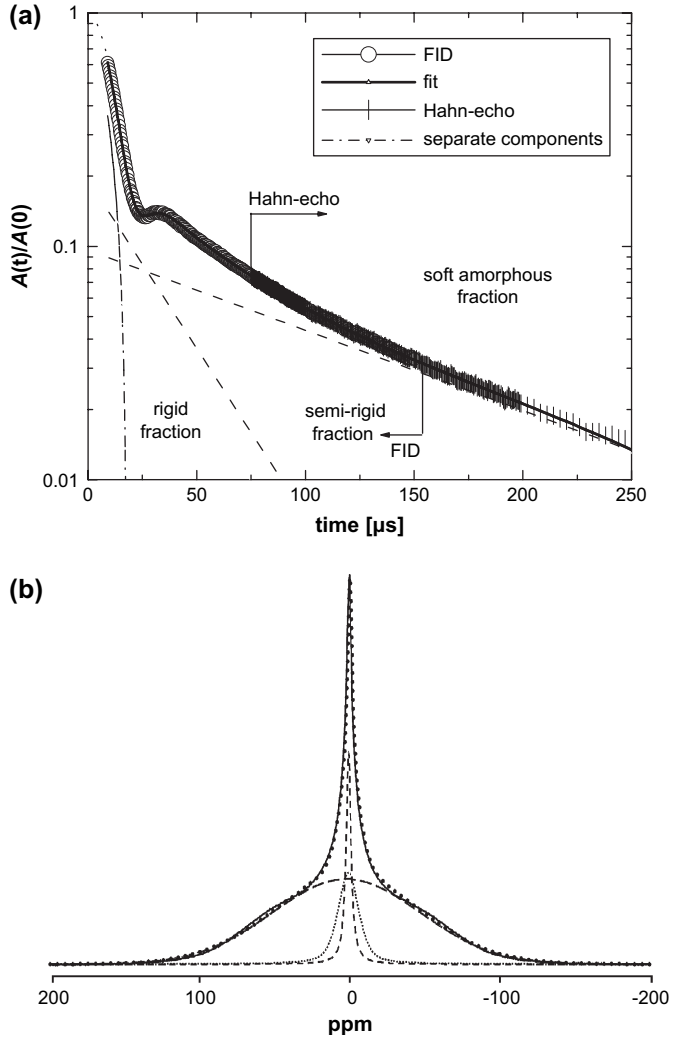

Fig. 6. (a) The decay of the transverse magnetization relaxation (points) for HDPE at 100 °C. The decay was measured at 20 MHz using the SPE (O) and HEPS (I) methods. The solid line represents the result of a least-squares fit of the decay with a linear combination of the Abragam function and two exponential functions. Dotted lines show the separate components that are assigned to HDPE fractions, which reveal distinct differences in molecular mobility. (b) Proton wide-line NMR spectra (solid line) measured at 500 MHz for HDPE at 100 °C. The dashed and dotted lines show the spectral components that are assigned to the rigid, semi-rigid, and soft fractions of HDPE – broad, intermediate, and narrow line widths, respectively.

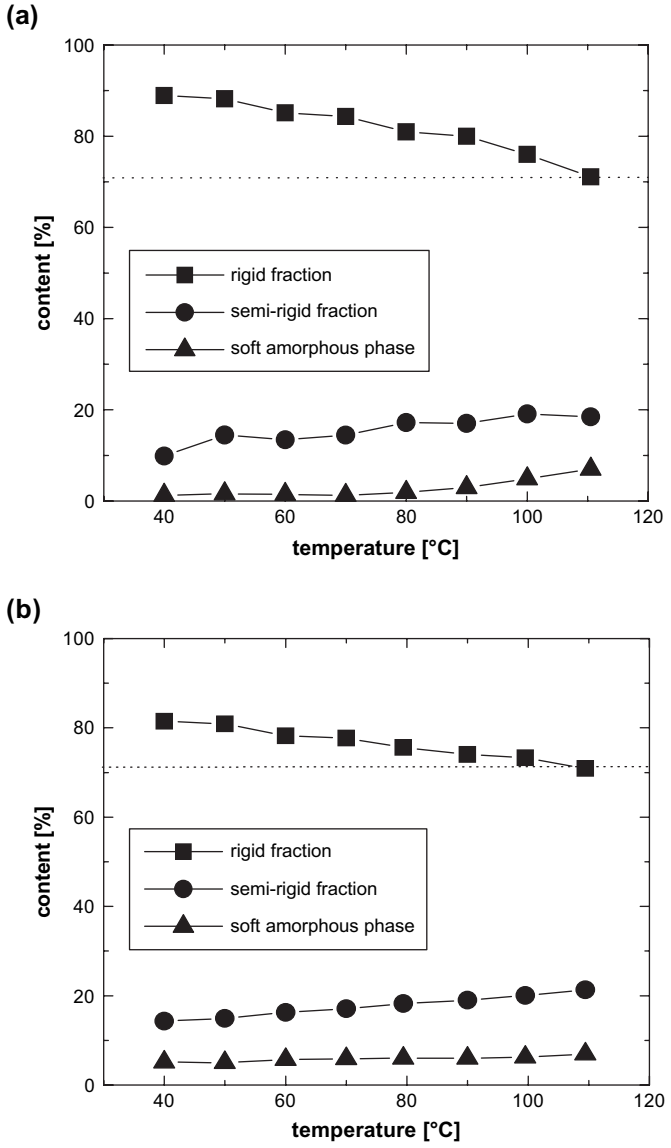

Fig. 7. Temperature dependence of the amount of rigid, semi-rigid, and soft fractions of HDPE measured with (a) low-field and (b) high-field NMR spectrometers. Dotted line shows crystallinity that was determinated by SAXS in the temperature range from 30 °C to 90 °C.

temperature at the time scale of the NMR experiment, i.e. in the range of 10^{-4}–10^{-5} s. The T_g of the HDPE sample that was determined by a high performance DSC equals −57 °C. The NMR T_g should be observed in the temperature range from −30 °C to −10 °C. Therefore, a proper choice of the temperature of the NMR experiment is required. (2) Since the T_2-relaxation experiments should be performed at temperatures well above T_g, the sample exposure to elevated temperatures can cause irreversible changes in the phase composition and thus in the molecular mobility. Therefore, the temperature for the experiments should not be too high to prevent annealing of the sample during the NMR experiment.

In order to find the optimum temperature for determinating the phase composition by NMR, we recorded the temperature dependence of the T_2 relaxation and the wide-line spectra (Fig. 7). At room temperature, a significant fraction of the amorphous phase is rigid at the time scale of the NMR experiments and this amorphous fraction contributes to the intensity of the broad line of the NMR spectra and the short T_2-relaxation component of FID, as can be concluded by comparing the amount of the rigid fraction with the crystallinity determined by SAXS, i.e. 71 ± 5 wt%. Upon increasing temperature, the amount of the rigid fraction, which is composed of the crystalline phase and the rigid fraction of the amorphous phase, gradually decreases, whereas the amount of the semi-rigid and soft fractions increases. These changes are caused by an increase in molecular mobility of the less constrained chain fragments in the amorphous phase, and possibly by melting of thin lamellae, which are inserted into the primary stack of crystallites

upon cooling of HDPE which was crystallized at elevated temperatures [51]. In the temperature range from approximately 100 °C to 120 °C, the amount of rigid fraction ($\%T_2^s$) is close to the crystallinity measured by SAXS. Above 120 °C, the amount of the rigid fraction decreases by melting. The DSC analysis of this sample shows that the extrapolated onset temperature of melting, as determined by a method described elsewhere [52] is in proximity of 125 °C and the peak of melting is observed at 136 °C. Thus, the temperature range from 100 °C to 110 °C is the most suitable for an accurate determination of the phase composition in HDPE, since (1) the largest differences in molecular mobility in the different fractions of HDPE is observed at these temperatures, (2) no substantial sample annealing occurs as will be shown below, and (3) the amount of the rigid fraction of HDPE does not largely depend on temperature and its value is close to crystallinity determined by SAXS. It is mentioned in this context that, in general, different methods for determination of crystallinity do not necessarily yield the same crystallinity value for exactly the same sample.

As far as the molecular mobility in HDPE is concerned, the changes in the T_2-relaxation times in the temperature range studied (Fig. 8) can be assigned to the following relaxation transitions in HDPE [53–56]. A small increase in T_2^s above 60–80 °C is related to chain motions in the crystalline phase – the α_c-relaxation process, which occurs prior to melting. Interpretation of the molecular mobility in the amorphous phase is more cumbersome. Despite numerous studies of relaxation processes in PE by different methods, molecular interpretation of the relaxation processes in the amorphous phase is under discussion [54]. The increase in T_2^l with increasing temperature from 40 °C to 70 °C can be associated with a relaxation process in the soft fraction of the amorphous phase. This temperature range and frequency of this relaxation, as estimated from change in T_2^l ($\approx$5–10 kHz), are in the range that is characteristic for the α_{am}-relaxation in the amorphous phase. It is noted that the α_{am}-relaxation in HDPE is very broad and hardly detectable by mechanical and dielectric relaxation methods [54]. Partial melting of HDPE crystals above 120 °C causes a decrease in constraints on chain motions in the amorphous phase and therefore an increase in molecular mobility in the amorphous phase, as reflected by an increase in T_2^i and T_2^l (Fig. 8).

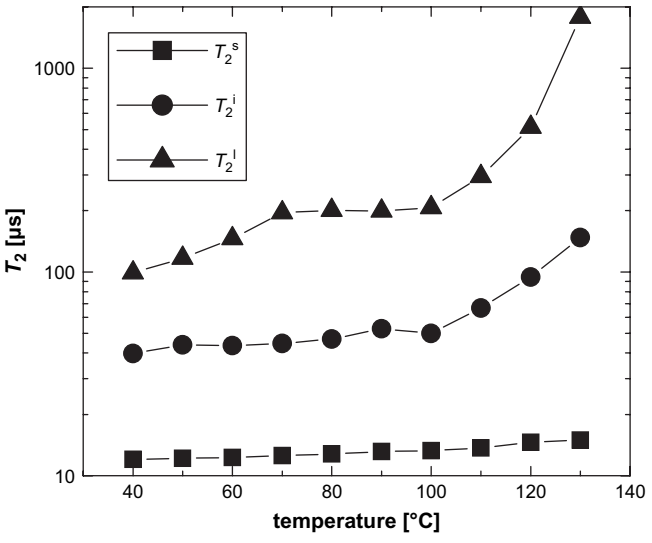

Fig. 8. Temperature dependence of ^{1}H T_2-relaxation times for HDPE. The relaxation components with short (T_2^s) intermediate (T_2^i), and long (T_2^l) decay time (see Fig. 6a) are assigned to the rigid, semi-rigid and soft fractions of HDPE, respectively.

3.3.2. The effect of annealing on molecular mobility and the phase composition

The experiments above have shown that the analysis of the phase composition should be preferably performed at elevated temperatures where the NMR parameters show enhanced difference. Since the NMR experiments take approximately 2 h, sample annealing is indeed an issue. In order to determine a temperature, at which no detectable changes in the relaxation will be observed during NMR experiments, the T_2 relaxation was recorded in real time at 100 °C, 110 °C and 121 °C. The data were recorded at 1 h intervals. Sample exposure to 100 °C and 110 °C for 60 h causes hardly any change in the molecular mobility and the phase composition. Annealing at 121 °C for 100 h shows an increase in the amount of the rigid fraction by 1 wt% at the expense of semi-rigid and the soft fractions of the amorphous phase (Fig. 9a). Due to annealing, both the melting temperature as well as the melting enthalpy increase, namely: the melting peak shifts from 139.1 °C to 145.4 °C, and the melting enthalpy increases from 232.8 J/g to 273.9 J/g. The molecular mobility in the rigid, semi-rigid and soft fractions of HDPE is also slightly affected by annealing at 121 °C (Fig. 9b). The value of T_2 for the rigid fraction (T_2^s) decreases upon annealing from 15 µs to 14 µs due to perfection of crystals, as it can be also concluded from large increase of the melting enthalpy at only 1 wt% crystallinity increase. The T_2-relaxation time for the semi-rigid fraction and soft amorphous phase decrease by a few percent. This decrease is likely to be caused by additional constraints imposed on to the amorphous phase due to the increased amount of crystalline phase.

The analysis of the temperature dependence of the T_2 relaxation and the annealing study show that 100 °C is the optimum temperature for quantitative analysis of the phase composition in HDPE using the NMR experiments. At this temperature, the relaxation components T_2^s, T_2^i and T_2^l (Fig. 8) largely originate from the crystalline phase, semi-rigid crystal–amorphous interface, and the soft fraction of the amorphous phase, respectively. The relative fraction of these components represents the corresponding weight fractions (Fig. 7a). The observation of three distinct T_2 relaxations rather than a wide distribution of the relaxation times indicates a fast loss of restrictions on rotational and translational chain mobility when moving away from the crystalline phase to the interface and to the soft fraction of the amorphous phase. Therefore, a stepwise change in the molecular mobility at the position between different phases is observed. Thus, we can conclude that the three-phase model describes well the phase structure of HDPE [11–15].

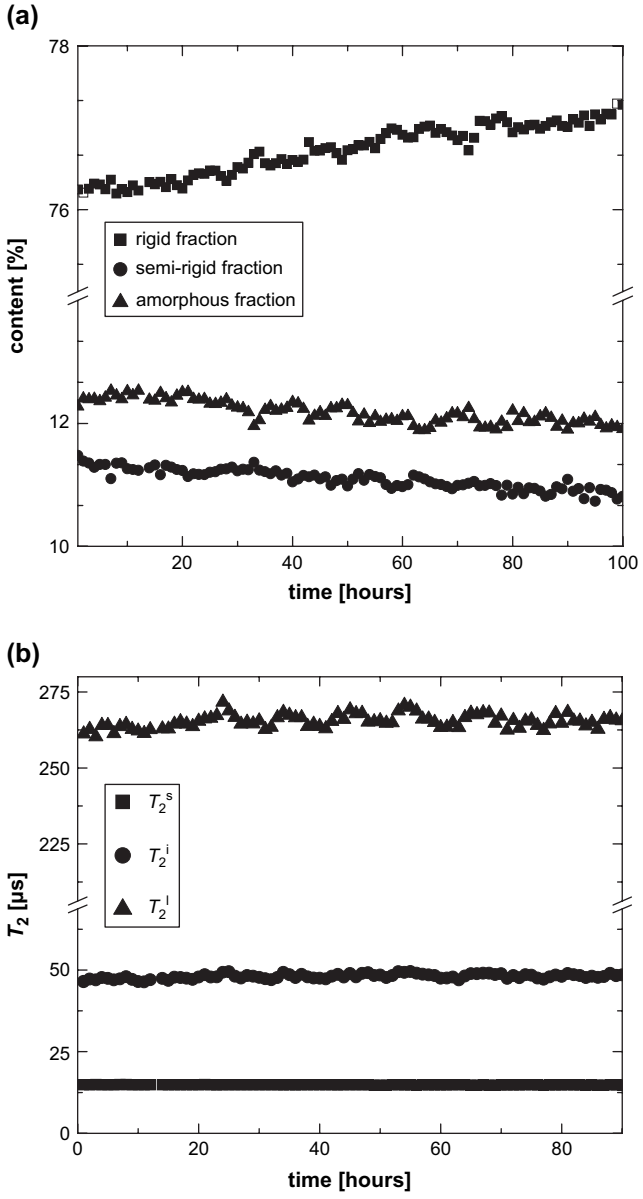

Fig. 9. (a) The amounts of crystalline phase ($\%T_2^s$), semi-rigid crystal–amorphous interface ($\%T_2^i$) and soft fraction of the amorphous phase ($\%T_2^l$) in HDPE as a function of the annealing time at 121 °C. (b) The effect of annealing on molecular mobility, as determined by the T_2-relaxation time for the different phases of HDPE. Larger the amplitude and/or frequency of molecular motions are, longer the T_2 value. The above relaxation characteristics are determined for the crystalline phase and the crystal–amorphous interface from the analysis of FID and using the Hahn-echo data for the soft fraction of the amorphous phase, as described in experimental part.

3.3.3. Thickness of domains by ^1H spin diffusion

An accurate analysis of the thickness of domains by NMR spin-diffusion experiments requires (1) an optimisation of a dipolar filter to obtain the highest selectivity to different phases (see Section 3.3.3.1), (2) knowledge of the spin-diffusion coefficients for modelling the experimental data (see Section 3.3.3.2), and (3) proper choice of a model that fits the morphology of the material studied. For a lamella morphology one-dimensional spin-diffusion model is the most suitable and applicable in the present study, as can be seen from the TEM picture in Fig. 3.

3.3.3.1. Double-quantum dipolar filter. The dipolar filter based on the excitation of the double-quantum coherences edits different dipolar spin networks as a function of the excitation/reconversion time τ (Fig. 2). Using the dipolar filter, different phases in HDPE can be selected by a proper choice of the excitation/reconversion time. This is an intrinsic property of the DQ coherences that are selectively excited for different phases upon increasing the excitation time depending on the strength of the dipolar couplings in a dipolar network in these phases [49,50]. The chain motions in the interface and mobile fraction reduce the strength of proton dipole–dipole interactions. Therefore, the DQ dipolar filter is highly sensitive to the heterogeneity of the dipolar network. This effect is enhanced by a difference in the rate of the transverse magnetization relaxation for hard and soft phases that affect the intensity of the DQ filtered NMR signals.

In order to determine the optimum τ value of the DQ filter (Fig. 2) [57], a DQ build-up curve was recorded. The DQ build-up curve for HDPE shows two maxima (Fig. 10). The first maximum is well defined and appears at a very short excitation time τ of approximately 10 μs. The second maximum is not so well defined and observed at an excitation time of about 25 μs. The efficiency of the filter is demonstrated in Fig. 11, which shows wide-line NMR spectra recorded with the DQ filter at different excitation/reconversion times τ. These spectra allow us to assign the maxima on the ^1H DQ build-up curve and to choose the optimum filter time for selecting the magnetization of the crystalline phase. At short τ values, the DQ filter edits only the signal of methylene groups with the strongest dipolar interactions, mainly in the crystalline phase. Since an isolated spin-1/2 pairs have a NMR spectrum with

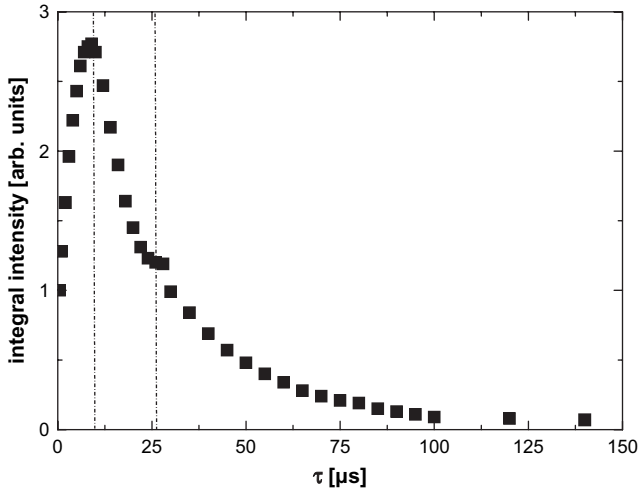

Fig. 10. Proton DQ build-up curve for HDPE at room temperature showing the dependence of the integral signal against the excitation time τ. The DQ build-up curve was measured with high-field NMR spectrometer. The maximum is observed at 10 μs and is marked by a dashed line. The low-intensity maximum at an excitation time of ≈25 μs largely originates from the semi-rigid fraction of HDPE.

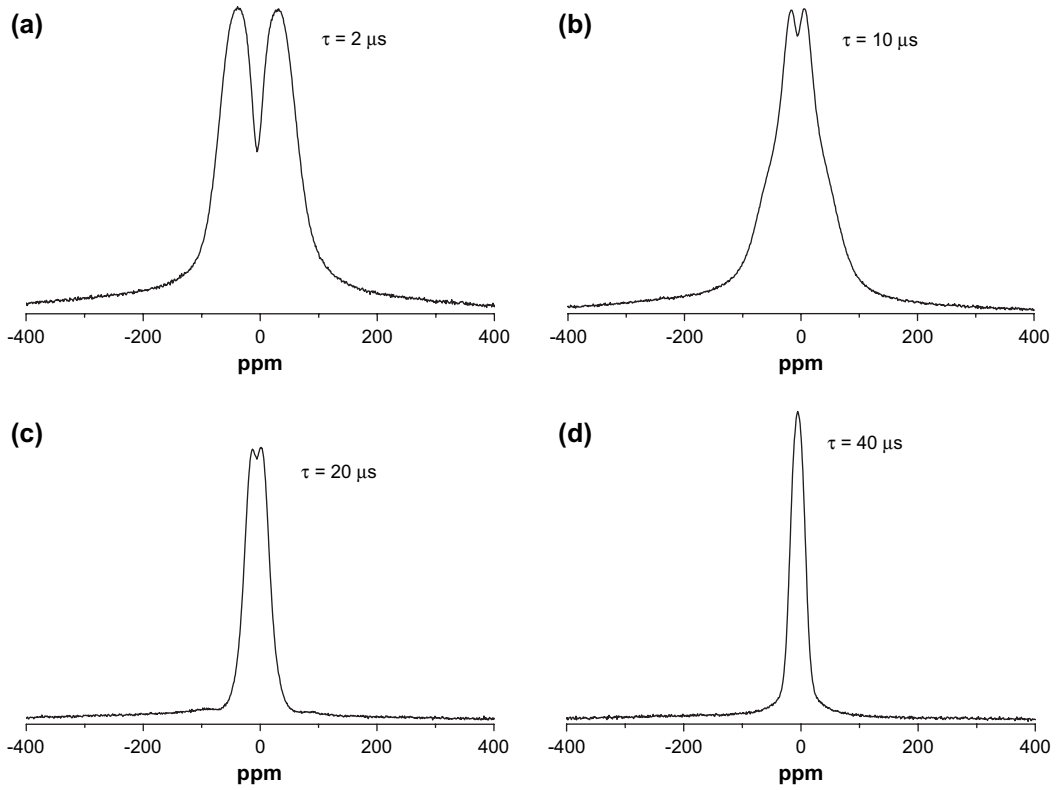

Fig. 11. High field proton wide-line NMR spectra of HDPE at room temperature recorded after different excitation/reconversion period in the DQ dipolar filter: $\tau = 2$ μs (a), $\tau = 10$ μs (b), $\tau = 20$ μs (c), and $\tau = 40$ μs (d). The spin-diffusion time t_d in the experiment (Fig. 2b) was set to 5 μs.

two peaks, the ^{1}H DQ filtered spectrum has the form of doublet (Fig. 11a) that is typical for CH_2 spin pairs in the crystalline surrounding of HDPE [12,14,15]. The broadening of the edited doublet is due to CH_2 intergroup dipolar interactions and the angular distribution of the dipolar couplings. Thus, at short excitation times ($\tau = 2-5$ μs) the filter selects mainly the magnetization from the rigid fraction of HDPE.

As the value of the excitation/reconversion time increases, the DQ filter still edits protons in the rigid region. However, it selects the dipolar network from intra- as well as intergroup dipolar coupled CH_2 groups. The resolution of the edited doublet is reduced by the dipolar broadening due to the methylene intergroup dipolar interactions. This is evident from the spectrum that is recorded at the excitation/reconversion times at 10 μs, which is around the maximum of the DQ build-up curve (Fig. 11b). Moreover, for this τ value, the DQ coherences of the methylene groups from the interfacial region are partially excited and contribute to the DQ filtered signals. An interesting property of the DQ filter is that it selects at long excitation times only the signal from the most mobile chain fragments in the amorphous phase (Fig. 11d) [32]. This is due to the fact that the FID from the rigid and interfacial regions decays to nearly zero during the free evolution of the single-quantum coherences in the five-pulse sequence. At intermediate filter time ($\tau \approx 20$ μs), the signal from the semi-rigid interfacial region is strongly enhanced (Fig. 11c). The line splitting for the interface of 20 kHz is apparently due to residual chain order in the interfacial layer, which is intermediate between that of the highly ordered crystalline phase and the disordered soft amorphous fraction [58,59]. Thus, the DQ filter shows high efficiency in selecting the magnetization of a particular HDPE domain with different molecular mobility. The high selectivity of the DQ filter is also observed in T_2 relaxation experiments at low resonance frequency (20 MHz). The excitation time of 5 μs is chosen to select the rigid fraction of HDPE in the spin-diffusion experiment both at high and low proton resonance frequencies.

3.3.3.2. Temperature dependence of spin diffusivities in HDPE. The values of the spin-diffusion coefficients should change with increasing temperature due to an increase in molecular mobility. Therefore, the spin-diffusion coefficients should be determined at different temperatures for accurate analysis of domain sizes in HDPE as a function of temperature.

The values of the spin-diffusion coefficients D for the rigid and the soft fractions of HDPE can be determined assuming, to a good approximation, that the NMR line shapes of the rigid and soft fractions are Gaussian and Lorentzian, respectively. The spin-diffusion coefficients can be related to the second van Vleck moment of the NMR absorption lines, which, in turn, is related to the full line width $\Delta\nu_{1/2}$ at half height. The presence of more intense chain motions in soft fraction averages proton residual dipolar couplings and reduces the value of the spin diffusivity. Hence, the spin diffusivity for the rigid (D_r) and soft (D_a) fractions is as follows [46]:

$$D_r \approx \frac{1}{12}\sqrt{\frac{\pi}{2\ln 2}}\langle r^2\rangle \Delta\nu_{1/2} \tag{7}$$

and

$$D_a \approx \frac{1}{6}\langle r^2\rangle \left[\alpha \Delta \nu_{1/2}\right]^{1/2}, \quad (8)$$

where $\langle r^2\rangle$ is the mean square distance between the nearest spins and α is a cut-off parameter for the Lorentzian line shape [46]. This cut-off parameter is introduced to specify the frequency range around the maximum value of the Lorentzian line needed to evaluate an effective second van Vleck moment. The temperature dependence of $\Delta\nu_{1/2}$ is determined at each temperature by spectral deconvolution as shown at one temperature in Fig. 6b. For calculating $\langle r^2\rangle$ the Discover program (version 2004.1) was used. The estimated weighted mean square of these distances $\langle r^2\rangle$ equals approximately 0.0484 nm^2. Since the conformer stereo structure evaluated from Discover program is difficult to obtain at different temperatures for the HDPE fractions, $\langle r^2\rangle$ value of 0.0484 nm^2 is taken as an average value for different HDPE fractions and temperatures. The semi-rigid fraction of HDPE has molecular mobility that is intermediate between that in rigid and soft fractions (Fig. 7). Therefore, an arithmetic average value of the spin-diffusion coefficients for rigid and soft fractions of HDPE was taken as the spin-diffusion coefficient of the semi-rigid fraction (D_i).

The calculated spin-diffusion coefficients are plotted as a function of temperature in Fig. 12. The values of the spin-diffusion coefficients decrease with increasing temperature due to an increase in the amplitude and the frequency of the chain motions in each fraction of HDPE. The increase in the chain mobility causes more efficient averaging of the proton dipole–dipole interactions and reduces the efficiency of the spin diffusion. Therefore, the determination of the spin-diffusion coefficient for each phase as a function of temperature is necessary for an accurate analysis of domain sizes.

3.3.3.3. The thickness of domains in HDPE. The spin-diffusion experiments were performed for HDPE at 70 °C, 100 °C and 120 °C before and after annealing for 100 h at 121 °C. Proton wide-line NMR spectra at three different spin-diffusion times t_d are shown in Fig. 13. At short t_d mainly the rigid fraction of HDPE is observed, as can be seen in Fig. 11a. Upon increasing the spin-diffusion time, the relative intensity of the rigid fraction in the spectra decreases and the intensity of the narrow line that originates from the soft amorphous fraction increases (Fig. 13). A similar behaviour is

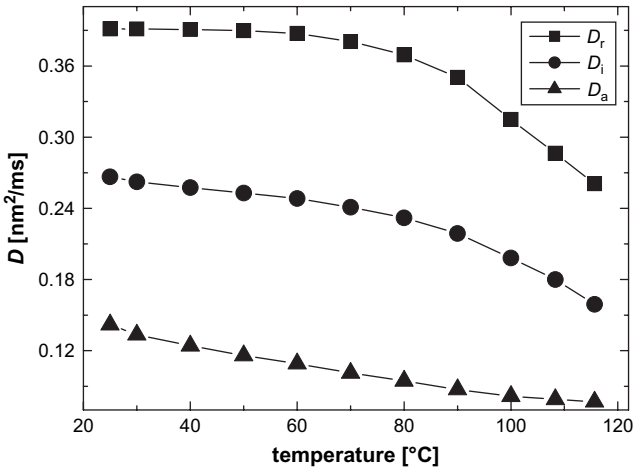

Fig. 12. The temperature dependence of the spin-diffusion coefficients D_r, D_i, and D_a for rigid, semi-rigid and soft fractions of HDPE, respectively.

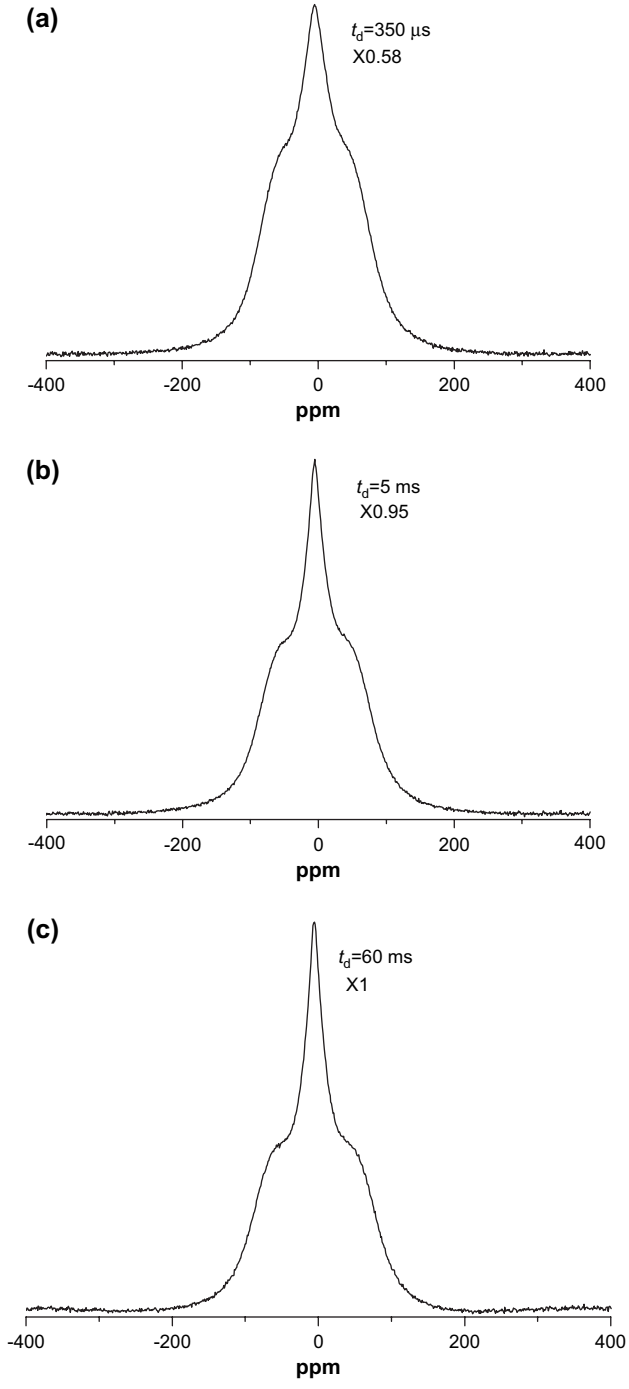

Fig. 13. Proton wide-line NMR spectra for HDPE at room temperature. The spectra were recorded using the spin-diffusion experiment, which is shown in Fig. 2, with different spin-diffusion time: (a) $t_d = 350$ µs, (b) $t_d = 5$ ms and (c) $t_d = 60$ ms.

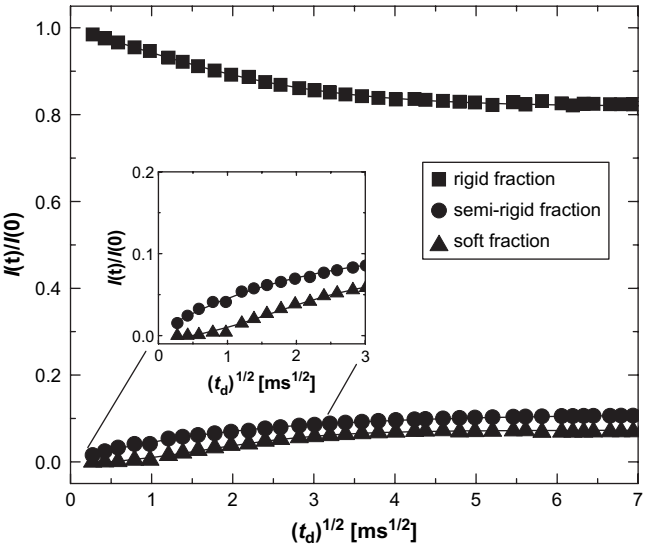

Fig. 14. Proton spin-diffusion data for the rigid (■), semi-rigid (●), and soft fractions (▲) of HDPE at 100 °C. The experiment was performed on a low-field NMR spectrometer. The normalized intensities of different fractions $I(t)/I(0)$ are obtained from Eq. (6). The solid lines are the best fit with 1D solutions of spin-diffusion equations [39]. The data of short t_d are shown in the inset.

observed in the time-domain experiments performed with the low-field NMR spectrometer.

The time evolution of the nuclear magnetization with increasing spin-diffusion time is shown in Fig. 14 for the rigid, semi-rigid and the soft fractions at HDPE before annealing. The magnetization flows from the rigid/crystalline phase to the semi-rigid interfacial layer and then reaches the soft fraction of the amorphous phase after some delay (see inset of Fig. 14). Already the visual analysis of the data reveals that the rigid and soft fractions of HDPE are separated by a layer with intermediate molecular mobility.

In order to determine the size of the domains with different molecular mobility, the spin-diffusion curves were fitted with equations that have been obtained using analytical solutions of the spin-diffusion equation for three distinct phases characterized by different spin diffusivity [39]. The spin-diffusion curve represents the changes in the experimental parameters given by the normalized amplitudes of the fitted transverse magnetization relaxation or NMR spectra as a function of the spin-diffusion time t_d (cf. Fig. 2). The explicit solutions of the spin-diffusion equations are complex and are reported in Ref. [39]. The spin-diffusion coefficients used in the calculation are those from Fig. 12. The values of the proton densities for the different phases of HDPE, which are required for the calculation [39], are determined from the densities of crystalline and amorphous phases of HDPE, i.e. $\rho_c = 0.99$ g/cm^3 and $\rho_a = 0.87$ g/cm^3. It is suggested that the density of the interface, $\rho_i = 0.93$ g/cm^3, is the mean value of the densities for the crystalline and amorphous phases.

The thickness of HDPE domains before annealing was determined using the time-domain and the frequency-domain spin-diffusion experiments, both methods yielding results that are in good agreement to each other (Table 1). The result

Table 1
The thickness of rigid (d_c), semi-rigid (d_i) and soft domains (d_a) at different temperatures in non-annealed HDPE[a,b]

The thickness of domains (nm)	Temperature (°C)		
	70	100	120
d_c	18.0 (19.0)	17.0 (17.0)	13 (12.5)
d_i	1.1 (1.1)	1.3 (1.4)	1.2 (1.3)
d_a	0.6 (0.5)	0.7 (0.8)	1.0 (1.1)
Long period from NMR: $\sum d = d_c + 2d_i + d_a$	20.8 (21.7)	20.3 (20.6)	16.4 (16.2)

The domain thickness was obtained from ^{1}H spin-diffusion experiments with a DQ filter.
[a] Measured using 500 MHz and 20 MHz (in brackets) NMR spectrometers.
[b] The relative error of the data is estimated to about 15%.

for long period is almost constant below 100 °C (Fig. 15a). Moreover below 100 °C, the thickness of the rigid fraction d_r slightly exceeds the lamella thickness determined by TEM and SAXS. This is due to the fact that the interfacial layer with intermediate mobility on the lamellae surface is largely immobilized below 100 °C, as can be seen by comparing the amount of the rigid fraction with the sample crystallinity measured by SAXS (Fig. 7). The thickness of the rigid domain slightly decreases with increasing temperature and at approximately 100 °C reaches the lamella thickness as measured by TEM and SAXS, i.e. 16–18 nm. Thus, the thickness of rigid domains at 100 °C represents lamellae thickness. The lamellae thickness at 120 °C is smaller than that at 100 °C, which could be caused by partial melting of the sample. Moreover, fragmentation of lamellae upon melting could also cause apparent decrease in lamellar thickness due to an increase in the efficiency of the spin diffusion. As far as the soft domain is concerned, its thickness increases with increasing temperature at the expense of rigid domains. The thickness of the interface is nearly constant in the studied temperature range and equals with 1.1–1.3 nm (Fig. 15c). This value is in the same range as previously estimated by Monte Carlo simulations interface thickness [58–60]. The simulations have shown that density, orientational order and transverse structure parallel to the lamella surface change from those of crystalline phase to disordered amorphous phase within a layer of 1.0–1.2 nm thickness that is adjacent to the lamellae surface. It should be noted that the interface thickness is close to the length of the statistical segment for PE chains, which consist of ≈7 carbon–carbon bonds [61] and equals to 0.8 nm for fully extended PE chain. Therefore, distinct differences in chain mobility in different fractions of HDPE are apparently caused by short-range correlations of chain motion due to the short length of statistical segment.

3.3.4. The effect of annealing on the thickness of domains

In order to determine the effect of annealing on the thickness of the rigid, semi-rigid, and soft domains, a compression-moulded HDPE plate was annealed at 121 °C for 100 h. The thickness of domains was determined at 70 °C, 100 °C and 120 °C and the results for the annealed sample are compared

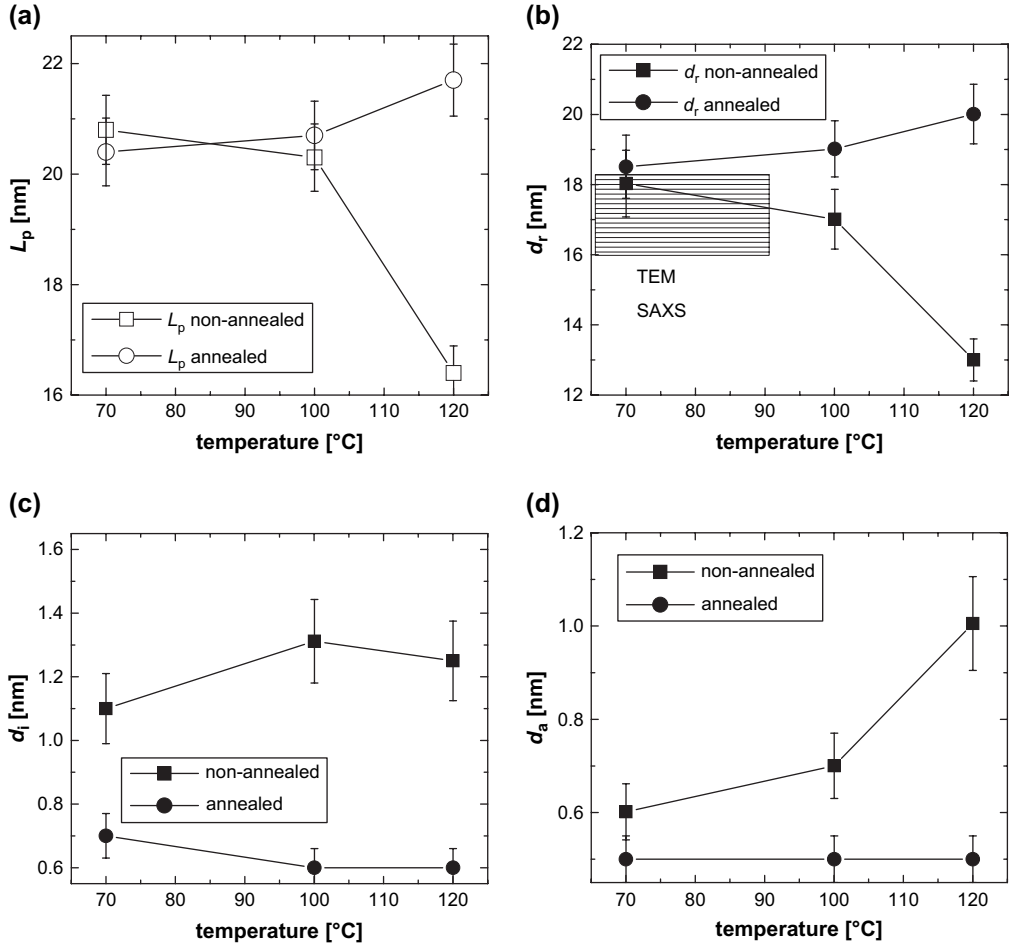

Fig. 15. The temperature dependence of the long period from NMR (a), the thickness of rigid (b), semi-rigid (c), and soft (d) domains of HDPE. The experiments were performed on low-field NMR spectrometer for a compression-moulded plate before and after annealing at 121 °C for 100 h. Shade area shows the lamellar thickness measured by NMR and TEM for non annealed samples.

with those of the non annealed sample (Fig. 15). Annealing causes a significant decrease in the thickness of the interfacial layer and the soft amorphous phase, and an increase in the lamellar thickness, which can clearly be seen for the results measured at 120 °C. The annealing causes only minor changes in molecular mobility (Fig. 9b).

The annealing study suggests the following mechanism of morphological changes due to annealing at elevated temperatures. Upon approaching the melting temperature, the molecular mobility increases both in the amorphous regions, the crystal–amorphous interface, and in the crystalline phase (α-relaxation) (Fig. 8). Previous ^{13}C NMR studies have suggested two types of crystalline environments with distinctly different molecular mobility: the more perfect one and that with defects [22,27]. It might be suggested that chain mobility increases at elevated temperatures in the less ordered, surface layer of lamellae, as it follows from a decrease in the lamella thickness above 100 °C for non-annealed sample (Fig. 15b). An increase in the molecular mobility is accompanied by partial melting of small crystals and less ordered fragments of the lamellae. An increased mobility in the amorphous phase and chain diffusion in- and out of the crystals (α-relaxation) [24] facilitate to some extent morphological changes towards a more thermodynamically stable, better-ordered crystalline structures and thicker lamellae. It should be mentioned in this respect that the root-mean-square displacement of chains in PE lamellae amounts to more than 10 nm at 100 °C within 100 s [24]. Chain rearrangements upon prolonged annealing at 121 °C for 100 h result in a decrease in molecular mobility in the crystalline phase, as it follows from a slight decrease of T_2^s during annealing and large increase in the melting enthalpy (from 232.8 J/g to 273.9 J/g) at only 1 wt% increasing in the crystallinity (Fig. 9b). These might suggest perfectioning of the crystalline order. Lamellae thickening and a slight increase in the crystallinity would cause additional slippage of chain entanglements towards the inner part of inter-lamellar amorphous regions causing additional immobilization of the soft fraction of the amorphous phases, as it can be concluded from the decrease of the thickness of this layer (Fig. 15c) and decrease in T_2^l (Fig. 9b). Thus, our observations reveal that annealing is accompanied by a continuous shift of the crystal–amorphous interface towards the inner part of the amorphous regions and reducing the thickness of the amorphous layer [23,62–64].

4. Conclusions

The effects of temperature and annealing on the following molecular and morphological characteristics of HDPE were studied by time- and frequency-domain proton solid-state NMR: (i) the amount of rigid, semi-rigid, and soft fractions of HDPE, (ii) the thickness of the domains with different molecular mobility and (iii) the molecular mobility in these domains.

This study was focused on two areas, namely (1) the improvement of solid-state NMR methods for determining the thickness of domains in heterogeneous polymers and (2) a better understanding of the phenomena that occur upon annealing of HDPE.

(1) The novel spin-diffusion experiments that are based on the double-quantum dipolar filter provided reliable information about the thickness of lamellae, crystal–amorphous interface and soft fraction of the amorphous phase. The applied method allows a better discrimination between the HDPE phases and, therefore, a more accurate analysis of the thickness of the domains. In order to improve accuracy of the method, the temperature dependence of the spin diffusivities in all three phases was determined, which allowed us to obtain reliable information about changes in the domain thickness as a function of temperature. The lamellar thickness and the long period determined by NMR are in good agreement with the results of classical methods, i.e. TEM and SAXS, which prove the reliability of the NMR method. This study has also shown that spin-diffusion experiments with advanced dipolar filters can be performed with a low cost, low-field NMR spectrometer, which broadens the range of applications of this equipment.

(2) This study shows that the three-phase model is the most appropriate description of the phase composition in HDPE. The spin-diffusion experiments show that rigid and soft fractions of HDPE are separated by a thin layer with intermediate molecular mobility. The thickness of this interface is nearly constant in the temperature range from 70 °C to 120 °C and its value is comparable to the length of the statistical segment of PE chains. This suggests that the interfacial layer largely originates from constraints on rotational and translational motions of chain fragments adjacent to the lamellae surface.

The crystalline phase, the semi-rigid crystal–amorphous interface, and the soft fraction of the amorphous phase exhibit a larger difference in molecular mobility at temperatures above 90 °C. Upon increasing the temperature, the molecular mobility begins to increase in the inner/softer part of the amorphous phase towards the lamellae surface. Annealing causes a significant decrease in the thickness of the interfacial layer and the soft amorphous phase, and an increase in the lamellar thickness. It is suggested that annealing is accompanied by structural reorganizations at the frontier between the crystalline and amorphous phases, and these reorganizations are largely influenced by the chain dynamics in the crystalline and amorphous phases. Annealing leads to improving perfections at a crystalline order (presumably in a layer close to the lamellae surface), and a continuous shift of the interface towards the inner part of the amorphous regions reducing the thickness of the soft amorphous layer. These observations are in agreement with a previously proposed mechanism of partial melting and surface crystallization upon annealing of HDPE at premelting temperatures [64].

Acknowledgements

This study was sponsored by SABIC Europe BV and the Resolve Department of DSM Research. C. Hedesiu gratefully acknowledges SABIC Europe BV for a PhD grant. The authors are grateful to Wilma Gijsbers for providing the TEM picture and Geert van den Poel for the high performance DSC results.

References

[1] Popli R, Mandelkern L. J Polym Sci Polym Phys Ed 1987;25:441–9.
[2] Mandelkern L, Peacock AJ. Stud Phys Theor Chem 1988;54:201–17.
[3] Flory PJ, Yoon DY. Nature 1978;272:226–9.
[4] Mandelkern L. Acc Chem Res 1990;23:380–94.
[5] Isasi JRL, Mandelkern MJ, Galante Alamo RG. J Polym Sci Polym Phys Ed 1999;37:323.
[6] Hirschinger J, Miura H, English AD. Macromolecules 1990;23:2153.
[7] Iwata K. Polymer 2002;43:6609.
[8] Hiss R, Hobeika S, Lynn C, Strobl G. Macromolecules 1999;32:4390.
[9] Schmidt-Rohr K, Spiess HW. Multidimensional solid-state NMR and polymers. London: Academic Press; 1994.
[10] Uehara H, Yamanobe T, Komoto T. Macromolecules 2000;33:4861–70.
[11] Bergmann K. J Polym Sci Polym Phys Ed 1978;16:1611.
[12] Fedotov VD, Abdrashitiva NA. Polym Sci USSR 1985;27:287.
[13] Eckman RR, Henrichs PM, Peacock AJ. Macromolecules 1997;30:2474.
[14] Hansen EW, Kristiansen PE, Pedersen B. J Phys Chem B 1998;102:5444.
[15] Kristiansen PE, Hansen EW, Pedersen B. J Phys Chem B 1999;103:3552.
[16] Kakudate T, Kakizaki M, Hideshima T. J Polym Sci Polym Phys Ed 1985;23:787.
[17] Ito M, Kanamoto T, Tanaka K. Macromolecules 1981;14:1779.
[18] Litvinov VM, Penning JP. Macromol Chem Phys 2004;205:172, and ref. therein.
[19] Litvinov VM, Soliman M. Polymer 2005;46:3077, and ref. therein.
[20] Litvinov VM, Mathot VBF. Solid State Nucl Magn Reson 2002;22:218.
[21] Kitamaru R, Horii F, Zhu Q, Bassett DC, Olley RH. Polymer 1994;35:1171.
[22] Hillebrand L, Schmidt A, Bolz A, Hess M, Veeman W, Meier RJ, et al. Macromolecules 1998;31:5010.
[23] Cheng J, Fone M, Reddy VN, Schwartz KB, Fisher HP, Wunderlich B. J Polym Sci Part B Polym Phys 1994;32:2683.
[24] Schmidt-Rohr K, Spiess HW. Macromolecules 1991;24:5288.
[25] Klein PG, Driver MAN. Macromolecules 2002;35:6598.
[26] Kuwabara K, Kaji H, Tsuji M, Horii F. Macromolecules 2000;33:7093.
[27] Hu JZ, Wang W, Bai S, Pugmire RJ, Taylor GMV, Grant DM. Macromolecules 2000;33:3359.
[28] Hentschel D, Sillescu H, Spiess HW. Polymer 1984;25:1078.
[29] McBrierty VJ, Packer KJ. Nuclear magnetic resonance in solid polymers. Cambridge: Cambridge University Press; 1993.
[30] Packer KJ, Pope JM, Yeung RR. J Polym Sci Polym Phys Ed 1984;22:589–616.
[31] Hu W-G, Schmidt-Rohr K. Polymer 2000;41:2979.
[32] Buda A, Demco DE, Bertmer M, Blümich B, Litvinov VM, Penning JP. J Phys Chem B 2003;107:5357.
[33] Buda A, Demco DE, Blümich B, Litvinov VM, Penning JP. Chem Phys Chem 2004;5:876–83.
[34] VanderHart DL, McFadden GB. Solid State Nucl Magn Reson 1996;7:45–66.

[35] Axelson DE, Mandelkern L, Popli R, Mathieu P. J Polym Sci Polym Phys Ed 1983;2:2319.
[36] Kitamaru R, Horii F, Murayama K. Macromolecules 1986;19:636.
[37] Kristiansen PE, Hansen EW, Pedersen B. Polymer 2000;41:311.
[38] Tanzer CI, Roy AK. In: Proceedings of the SPE ANTEC '95, vol. 2. Boston, MA, USA; 1995. p. 2700.
[39 Buda A, Demco DE, Bertmer M, Blümich B, Reining B, Keul H, et al. Solid State Nucl Magn Reson 2003;24:39.
[40] Ba Y, Ripmesster JA. J Chem Phys 1998;108:8589–94.
[41] Cherry BR, Fujimoto CH, Cornelius CJ, Alam TM. Macromolecules 2005;38:1201–6.
[42] Vonk CG. J Appl Crystallogr 1973;6:149.
[43] Feigin LA. Structure analysis by small-angle X-ray and neutron scattering. New York; 1987.
[44] Abragam A. The principles of nuclear magnetism. Oxford: Clarendon Press; 1961.
[45] Clauss J, Schmidt-Rohr K, Spiess HW. Acta Polym 1993;44:1–17.
[46] Demco DE, Johansson A, Tegenfeldt J. Solid State Nucl Magn Reson 1995;4:13–38.
[47] Idiyatullin DSh, Khozina EV, Smirnov VS. Solid State Nucl Magn Reson 1996;7:17.
[48] Assink RA. Macromolecules 1978;11:1233.
[49] Munowitz M, Pines A. Adv Chem Phys 1987;66:1–152.
[50] Ernst RR, Bodenhausen G, Wokaun A. Principles of nuclear magnetic resonance in one and two dimensions. Oxford: Clarendon; 1987.
[51] Strobl GR, Schneider MJ, Voigt-Martin IG. J Polym Sci 1980;18:1361.
[52] Mathot VBF. Calorimetry and thermal analysis of polymers. Munich, Germany, Vienna, New York: Hanser Publishers; 1994. p. 34–5.
[53] McCrum NG, Read BE, Williams G. Anelastic and dielectric effects in polymeric solids. New York: Wiley; 2004.
[54] Boyd RH. Polymer 1985;26:323.
[55] Wool RP. Macromolecules 1993;26:1564.
[56] Pavel S, Hashimoto T, Kenji S, Arkadiusz G. Polymer 2005;46: 513–21.
[57] Schneider M, Gasper L, Demco DE, Blümich B. J Chem Phys 1999;111: 402.
[58] Gautman S, Balijepalli S, Rutledge GC. Macromolecules 2000;33: 9136–45.
[59] Balijepalli S, Rutledge GC. Comput Theor Polym Sci 2000;10:103–13.
[60] Mandelkeren L, Aloma RG, Kennedy MA. Macromolecules 1990;23: 4721–3.
[61] Aharoni SM. Macromolecules 1983;16:1722–8.
[62] Matsuda H, Aoike T, Uehara H, Yamanobe T, Komoto T. Polymer 2001; 42:5013–21.
[63] Bassett DC, Carder DR. Polymer 1973;24:387.
[64] Strobl GR. The physics of polymers. Berlin: Springer-Verlag; 1997.